Electrostatic gating dependent multiple-band alignments in a high-temperature ferromagnetic $Mg(OH)_2/VS_2$ heterobilayer

Wenqi Xiong,[1] Congxin Xia,[1,*] Juan Du,[1] Tianxing Wang,[1] Xu Zhao,[1] Yuting Peng,[2] Zhongming Wei,[3,†] and Jingbo Li[3,‡]

[1]*College of Physics and Material Science, Henan Normal University, Xinxiang 453007, China*

[2]*Department of Physics, University of Texas at Arlington, Texas 76019, USA*

[3]*Institues of Semiconductors, Chinese Academy of Sciences, Beijing 100083, China*

(Received 4 January 2017; revised manuscript received 1 April 2017; published 9 June 2017)

Searching for ferromagnetic (FM) van der Waals (vdW) heterostructures with high Curie temperature and multiple-band alignments is crucial to develop next-generation spintronic and optoelectronic nanodevices. Here, through first-principles methods, the FM vdW heterostructure is found for the first time in the $Mg(OH)_2/VS_2$ heterobilayer with high Curie temperature (385 K) and type-II alignment. The negative electric field induces the transition from type-II to type-III alignment in the spin-up channel. However, under the positive electric field, the type-II to type-I alignment transition occurs in the spin-up and spin-down channels. This work provides the possibilities of realizing the high-temperature FM vdW heterostructures and electrostatic gating dependent multiple-band alignments in practice.

DOI: 10.1103/PhysRevB.95.245408

Recently, more and more two-dimensional (2D) materials with novel properties have been studied, such as graphene [1–3], transition metal dichalcogenides (TMDs) [4–7], and applied successfully in nanoelectronics and optoelectronic devices. However, most of 2D materials are intrinsically nonmagnetic in their pristine forms, which limits the development of next-generation nano-spintronic devices. Thus, introducing magnetism into the 2D nonmagnetic (NM) materials and searching for a new class of 2D ferromagnetic (FM) materials are crucial to achieve high-performance spintronic devices at room temperature [8,9].

More recently, the 2D atomically VS_2 monolayer is attracting intense attention due to its intrinsic FM semiconducting characteristics [10–14]. Huang *et al.* predicted that the VS_2 monolayer is a half semiconductor in which both electrons and holes share the same spin channel [15]. In addition, our recent studies also showed that the VS_2 monolayer can be switched from a half-semiconductor to a half-metal under a rather wide range of doping density [16]. The intriguing reports significantly expand the potential applications of 2D VS_2-based spintronic electronic devices.

To extend the applications of 2D VS_2 nanosheets in nanoelectronics and spintronics, it is very important to modulate the electronic structures, spin degree of freedom, and magnetism of the VS_2 nanosheets. According to previous studies, compared to a single-component 2D material, constructing the 2D materials-based van der waals (vdW) heterostructure is a very effective strategy to gain novel electronic and optoelectronic characteristics [17–20]. However, to our knowledge, there are rare reports on the 2D semiconducting VS_2-based vdW heterostructure. Therefore, in this work, we plan to combine a NM $Mg(OH)_2$ monolayer with a FM VS_2 monolayer to construct the $Mg(OH)_2/VS_2$ vdW heterostructure, exploiting its electronic structure, spin polarization, magnetism, and related promising applications in nanoelectronic and spintronic devices.

For a 2D $Mg(OH)_2$ monolayer, it was fabricated successfully from its layered bulk crystals and has a wide direct-gap with the value of 4.8 eV [21]. And studies also show that compared with 2D MoS_2 nanosheets, the 2D $Mg(OH)_2/MoS_2$ vdW heterostructure can achieve an obviously enhanced optical performance [21]. More recently, the first-principles calculations indicate that the $Mg(OH)_2/WS_2$ heterostructure presents a transition of heterostructure types under an external electric field [22]. In addition, the lattice constants of the $Mg(OH)_2$ and VS_2 monolayer are very close, which indicate that there is a slight lattice mismatch between $Mg(OH)_2$ and VS_2 and it is easy to construct the stacking heterostructure. Therefore, in this work, we carry out the theoretical studies on the band structure and magnetism of $Mg(OH)_2/VS_2$ vdW heterostructure using first-principles methods, considering electric field effects.

The structure relaxation and electronic structure calculation are carried out by using Vienna *ab initio* simulation package based on spin-polarized density functional theory (DFT) [23,24]. The exchange correlation potential is described with the Perdew-Burke-Ernzerhof (PBE) of the generalized gradient approximation (GGA) [25]. The projected argument wave (PAW) potential is used to describe the ion-electron potential [26]. Moreover, the electron plane wave function is expanded up to a cutoff energy of 500 eV. The Brillouin zone (BZ) integration is sampled using $15\times15\times1$ and $7\times7\times1$ Monkhorst-Pack k-point meshes for monolayer and heterostructure, respectively [27]. The geometry structures are fully relaxed until energy and forces are converged to 10^{-5} eV/atom and 0.01eV/Å, respectively. A vacuum region of more than 20 Å is performed to avoid the interaction caused by the periodic image. Meanwhile, a semiempirical DFT-D2 method is also used to give a good description of long-range weak vdW interactions [28,29]. The hybrid Heyd-Scuseria-Ernzerhof (HSE06) method is used to obtain the correct band structure [30,31]. To quantitatively characterize

*xiacongxin@htu.edu.cn

†zmwei@semi.ac.cn

‡jbli@semi.ac.cn

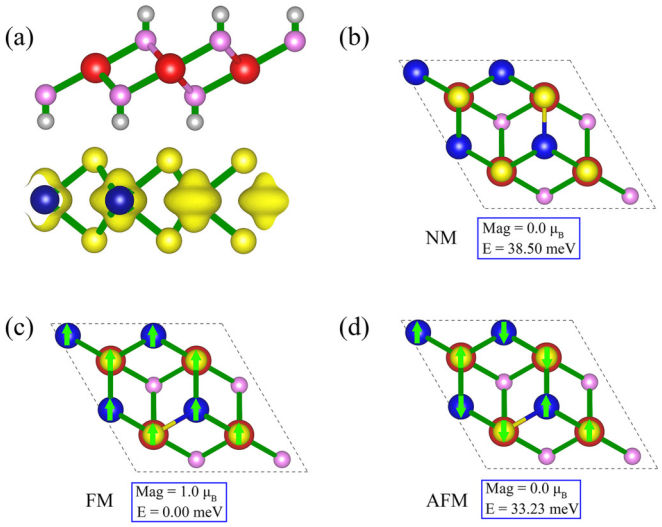

FIG. 1. (a) Spin densities of $Mg(OH)_2/VS_2$ heterostructure. (b) The NM, FM, and AFM configurations of the heterostructure, respectively. The grey, pink, red, yellow, and blue balls represent H, O, Mg, S, and V atoms, respectively.

the structural stability of $Mg(OH)_2/VS_2$ heterostructure, the binding energies E_b between $Mg(OH)_2$ and VS_2 monolayers are calculated as in Ref. [32],

$$E_b = E_{Mg/V} - E_{Mg} - E_V, \quad (1)$$

where $E_{Mg/V}$, E_{Mg}, and E_V are the total energies of the $Mg(OH)_2/VS_2$ heterostructure, the pristine $Mg(OH)_2$ and VS_2 monolayers, respectively.

In order to simulate the properties of $Mg(OH)_2/VS_2$ heterostructure, we firstly calculate the structural parameters and band structure (see the Supplemental Material for details [33]) of 2D $Mg(OH)_2$ and VS_2 monolayers, which agree with previous publications [13–15,21,22]. Then, we build the supercell model of $Mg(OH)_2/VS_2$ heterostructure by attaching the primitive cells of $Mg(OH)_2$ and VS_2 together, considering three kinds of different stacking patterns (see the Supplemental Material for details [33]). The small lattice mismatch of 0.48% can induce a slight change on the electronic structure of the heterobilayer. After the total energy and binding energy calculations (see Supplemental Material for details [33]), Fig. 1(a) presents the atomic configuration of $Mg(OH)_2/VS_2$ heterostructure with the binding energy of -117.8 meV per unit cell and the interlayer distance of 2.228 Å, which is lower than that of bilayer graphene (-31 meV per carbon atom).

To study the magnetic mechanisms of the $Mg(OH)_2/VS_2$ heterostructure, Fig. 1(a) plots the spin density of the heterostructure. It can be seen that the polarized charges mainly arise from the localized V atoms, while the contribution of other atoms is relatively small. Moreover, to check how the $Mg(OH)_2$ layer affects the magnetism of VS_2 monolayer, we employ a (2×2) supercell of $Mg(OH)_2/VS_2$ heterostructure to calculate the total energies of three different magnetic phases, i.e., NM, FM, and antiferromagnetic (AFM) states, as shown in Figs. 1(b)–1(d). Numerical results show that the total energy of the FM state is lower by 33.23 meV than that of the AFM state, indicating that the $Mg(OH)_2/VS_2$ heterostructure

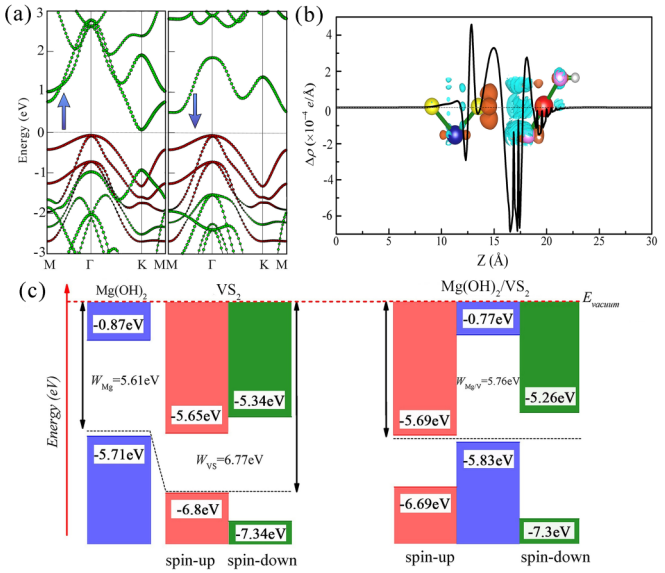

FIG. 2. (a) The projected band structure of $Mg(OH)_2/VS_2$ heterostructure with spin-up and spin-down bands. The sizes of the red and green colors represent the projected weight of $Mg(OH)_2$ and VS_2 components, respectively. (b) The plane-averaged charge density difference of $Mg(OH)_2/VS_2$ heterostructure at equilibrium distance along the z direction. The inset is the 3D surface of the charge density difference, the brown and cyan areas represent electron accumulation and depletion, respectively. (c) Band alignments and work functions of monolayers and heterostructure, referring to the vacuum level (E_{vacuum}).

still possesses the characteristics of the FM ground state. Meanwhile, we also calculate the energy difference between FM and AFM of VS_2 monolayer is 45.6 meV per unit cell, which is similar to the reported value of 44.2 meV [34].

In addition, for a stable FM material, high Curie temperature T_c is necessary and beneficial to the spintronics and related devices. Therefore, based on the mean-field theory and the Heisenberg model, we also estimate the Curie temperature T_c by using the following formula:

$$\gamma k_B T_c/2 = E_{AFM} - E_{FM}, \quad (2)$$

where γ and k_B are the coordinated numbers of the system and the Boltzmann constant [35], respectively. In this work, the coordinated number γ of the system is 2. The estimated Curie temperature T_c of the $Mg(OH)_2/VS_2$ heterostructure is 385 K. Therefore the novel magnetic properties of VS_2 can be maintained and a high Curie temperature can be also realized by stacking the $Mg(OH)_2$ on the VS_2 layers, implying that the $Mg(OH)_2/VS_2$ vdW heterostructure can be well applied to spintronics devices in practice.

To understand the underlying physics mechanisms of electronic structures of the heterostructure, in Fig. 2, we investigate the band structures, the band alignments, and the charge density difference of the $Mg(OH)_2/VS_2$ heterostructure. Figure 2(a) shows that for the spin-up band, the conduction-band maximum (CBM), and valence-band minimum (VBM) are located at K and Γ points, respectively, indicating that the majority band has an indirect band gap of 0.14 eV, while for the spin-down band, the CBM lies along the M-Γ line, while

the VBM remains at the Γ point, gaining an indirect band gap of 0.57 eV. Moreover, one can see from the projected band structure of Fig. 2(a) that in the $Mg(OH)_2/VS_2$ heterostructure, the hole states are localized in the NM $Mg(OH)_2$ layer, while the spin-polarized electron states come from the FM VS_2 layer, and the spin-up electron states have lower energies. Thus these results show that the $Mg(OH)_2$ layer can tune effectively the electron spin-polarization and exciton optical properties in the $Mg(OH)_2/VS_2$ heterostructure.

It is well known that the band alignments are significant for the physics and device applications of the semiconductor-based heterostructures. Thus, in Fig. 2(c), we calculate the band alignments of $Mg(OH)_2$, VS_2, and $Mg(OH)_2/VS_2$ heterostructure. Figure 2(c) shows that the work functions (the difference between the vacuum level and the Fermi level) of $Mg(OH)_2$ and VS_2 monolayers are 5.61 and 6.77 eV, respectively [22,34]. Moreover, the work function of $Mg(OH)_2/VS_2$ heterostructure is calculated to be 5.76 eV, which increases by 0.16 eV and diminishes by 1.01 eV with respect to the values of isolated $Mg(OH)_2$ and VS_2 monolayers, respectively. The reason is that when two layers touch, the spontaneous interlayer charge transfer induces Fermi level shifts upward and downward for $Mg(OH)_2$ and VS_2 layers, respectively, reaching a certain work function. In addition, Fig. 2(c) also shows that both spin phases (spin-up and spin-down) possess the type-II heterostructure, facilitating the separation of photo-excited electrons and holes [36]. Interestingly, we can also see that conduction-band offsets (ΔE_C, 4.92 and 4.49 eV) and valence-band offsets (ΔE_V, 0.86 and 1.47 eV) are observed for spin-up and spin-down channels, respectively. Therefore the different separation possibility of electrons and holes for spin-up and spin-down channels implies that the system has a great potential for effective spin manipulation and good performance in spintronic devices.

To visualize the charge redistribution and understand the charge transfer mechanism between $Mg(OH)_2$ and VS_2 layers in the heterostructure, in Fig. 2(b), we also calculate the plane-averaged charge density difference as $\Delta_\rho = \rho_{Mg/V} - \rho_{Mg} - \rho_V$, where $\rho_{Mg/V}$, ρ_{Mg}, and ρ_V are the charge densities of the heterostructure, $Mg(OH)_2$, and VS_2 layers, respectively. It can be seen from Fig. 2(b) that the charge is depleted on the $Mg(OH)_2$ side (blue area), while the charge is accumulated in the VS_2 side (red area), thus a remarkable charge rearrangement occurs at the interface of the hybrid structure. The behavior of charge redistribution often results in electron-hole puddles at the interface [37–39].

In experiment, the gating is an effective method to modulate the type of carriers and relative position of energy level to the Fermi level. Now we turn to investigate the external electric field effects on the electronic structures of $Mg(OH)_2/VS_2$ heterostructure. The positive electric field direction is defined from VS_2 to $Mg(OH)_2$. Figure 3(a) gives the evolution of the band gaps as a function of the external electric field. It is clearly shown that the band gaps of the heterostructure are highly sensitive to the external electric field. Moreover, the asymmetric variation of band gaps implies that a strong built-in electric field exists in the $Mg(OH)_2/VS_2$ heterostructure, which may be because a strong polarized surface exists in the $Mg(OH)_2$ layer in the heterostructure [21]. In addition, we can see from Fig. 3(a) that when we increase the strength

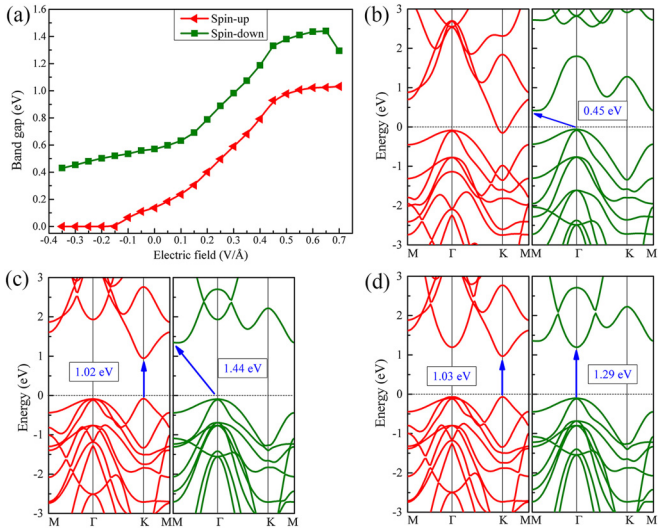

FIG. 3. (a) The spin-up and spin-down band gaps as a function of the electric field. The band structures of $Mg(OH)_2/VS_2$ heterostructure at various values of electric field: (b) −0.3, (c) 0.6, and (d) 0.7 V $Å^{-1}$, respectively.

of the negative electric field, the band gaps of spin-up and spin-down channels decrease monotonically. Moreover, the spin-up channel shows a semiconductor-metal transition at the electric field value of −0.15 V $Å^{-1}$, while the spin-down channel still retains semiconducting properties, for example, as shown in Fig. 3(b). Therefore the strong negative electric field can induce half-metallic states in the $Mg(OH)_2/VS_2$ heterostructure, which can provide a path to realize 100% spin-polarized currents in high performance spintronic devices [40,41].

Compared to the band gap variations in the negative electric field case, the positive electric field presents the opposite variation. Also, the spin-up and spin-down band gaps of the heterostructure increase monotonously with the increase of the positive electric field. When the positive electric field is further increased and exceeds 0.5 V $Å^{-1}$, the spin-up and spin-down band gaps increase slowly. Interestingly, in Fig. 3(c), the calculated band structures at an electric field of 0.6 V $Å^{-1}$ show that the spin-up band shows an indirect-direct band gap transition—the VBM is changed from Γ to K point—while the spin-down band maintains an indirect gap. At a larger electric field of 0.7 V $Å^{-1}$, a decrease of the spin-down band gap is observed. Meanwhile, the corresponding band structure indicates that the CBM shifts from M to Γ point under a positive electric field [see Fig. 3(d)]. Therefore a positive electric field can induce an indirect-direct transition and significantly improve the optical performance of the system in optoelectronics devices.

In order to further understand the electric field effects on the $Mg(OH)_2/VS_2$ heterostructure in Fig. 4, we show the band alignment of the $Mg(OH)_2/VS_2$ heterostructure for different external electric fields. It can be seen from the band alignment that the Fermi level monotonously drops from an electric field value of −0.3 to 0.7 V $Å^{-1}$, resulting in an increase of the work function. Meanwhile, the levels of CBM

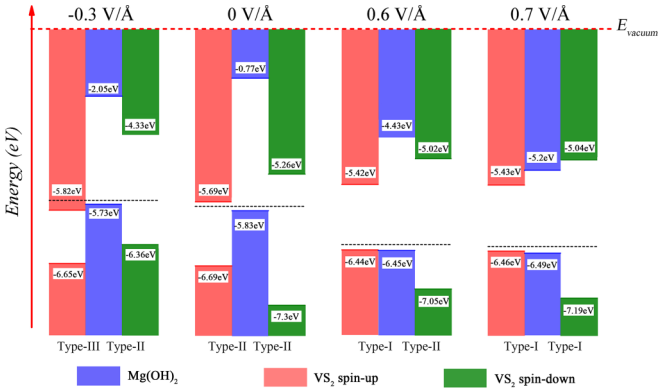

FIG. 4. Band alignments of $Mg(OH)_2/VS_2$ heterostructure at various electric field values: −0.3, 0, 0.6, and 0.7 V Å^{-1}, respectively, referring to the vacuum level (E_{vacuum}).

and VBM of $Mg(OH)_2$ and VS_2 components shift relative to the Fermi level, thus a heterostructure type transition is possible. Specifically, in the electric field of −0.3 V Å^{-1} case, the spin-down channel remains a type-II heterostructure while the spin-up channel presents a type transition from type-II to type-III. Moreover, the type-III heterostructure is demonstrated in tunneling field effect transistors (TFETs) to enhance the tunneling current density [42], which has been found in other nanomaterials [43,44]. Therefore the negative electric field successfully realizes the spin manipulation in the $Mg(OH)_2/VS_2$ heterostructure, i.e., the spin-up and spin-down channels have different application fields in nanoelectronics and spintronics.

When an electric field of 0.6 V Å^{-1} is applied, the spin-down channel is type-II heterostructure, while the spin-up channel is changed to a type-I heterostructure due to the form of a straddling gap [21]. The type-I heterostructure can facilitate the fast recombination of electrons and holes and is widely utilized in light-emitting diodes (LEDs) [45,46]. When we further increase the positive electric field, the CBM level of $Mg(OH)_2$ layer rapidly moves down and is well below that of the spin-down channel of the VS_2 layer, implying a type transition from type-II to type-I in the spin-down channel of the heterostructure. Based on this transition, both the spin-up and spin-down channels of $Mg(OH)_2/VS_2$ heterostructure possess the type-I heterostructure. Our findings reveal the possibility of electrostatic gating-induced tunable heterostructure type transitions in the heterostructure, which may be used in high-performance spintronic and optoelectronic devices.

Finally, we would like to point out that from a practical viewpoint, when electrostatic gating is applied, the effects of substrate need to be considered. Generally, a SiO_2 substrate is usually considered as substrate for experimental studies on most of 2D materials and related devices [47–49]. However, the theoretical studies show that the defect-free SiO_2 substrate does not affect significantly the electronic properties of monolayer MoS_2 due to their weak mutual interaction [50]. Moreover, experimental studies verify that the weak vdW interaction between graphene sheets and the SiO_2 substrates plays a negligible role [51]. In addition, recent studies reported that the $Mg(OH)_2/MoS_2$ heterostructure has also been experimentally fabricated on a SiO_2 substrate [21]. Here we only give the discussion about the effects from the substrate surface. In order to quantify the substrate effects on the 2D $Mg(OH)_2/VS_2$ heterostructures, further theoretical and experimental works are expected in future studies.

In conclusion, through first-principles calculations, we have demonstrated a new FM $Mg(OH)_2/VS_2$ vdW heterostructure with type-II alignment and high Curie temperature (385 K). Interestingly, an applied negative electric field induces a transition from type-II to type-III in the spin-up channel, while the spin-down channel remains a type-II heterostructure. In addition, when a positive electric field is applied, an indirect-direct gap transition and a type-II to type-I heterostructure transformation occur in both spin-up and spin-down channels. These results not only open up an opportunity to realize the FM type-II vdW heterostructure with high temperature, but also predicate the possibility of electrostatic gating-induced multiband alignments in the heterostructures, which are useful for next-generation multifunctional spintronic and optoelectronic devices.

This research was supported by the National Natural Science Foundation of China under Grants No. 11674084, No. 61622406, No. 11674310, No. 61571415, and No. 51502283. The calculations are also supported by The High Performance Computing Center of Henan Normal University.

[1] K. S. Novoselov, A. K. Geim, S. V. Morozov, D. Jiang, M. I. Katsnelson, I. V. Grigorieva, S. V. Dubonos, and A. A. Firsov, Nature (London) **438**, 197 (2005).
[2] A. K. Geim and K. S. Novoselov, Nat. Mater. **6**, 183 (2007).
[3] A. H. Castro Neto, F. Guinea, N. M. R. Peres, K. S. Novoselov, and A. K. Geim, Rev. Mod. Phys. **81**, 109 (2009).
[4] Y. Hao, L. Wang, Y. Liu, H. Chen, X. Wang, C. Tan, S. Nie, J. W. Suk, T. Jiang, T. Liang, J. Xiao, W. Ye, C. R. Dean, B. I. Yakobson, K. F. McCarty, P. Kim, J. Hone, L. Colombo, and R. S. Ruoff, Nat. Nanotechnol. **11**, 426 (2016).
[5] B. Radisavljevic, A. Radenovic, J. Brivio, V. Giacometti, and A. Kis, Nat. Nanotechnol. **6**, 147 (2011).
[6] H. Wang, L. Yu, Y.-H. Lee, Y. Shi, A. Hsu, M. L. Chin, L.-J. Li, M. Dubey, J. Kong, and T. Palacios, Nano Lett. **12**, 4674 (2012).
[7] H. S. Lee, S.-W. Min, Y.-G. Chang, M. K. Park, T. Nam, H. Kim, J. H. Kim, S. Ryu, and S. Im, Nano Lett. **12**, 3695 (2012).
[8] R. J. Green, T. Z. Regier, B. Leedahl, J. A. McLeod, X. H. Xu, G. S. Chang, E. Z. Kurmaev, and A. Moewes, Phys. Rev. Lett. **115**, 167401 (2015).
[9] T. Cao, Z. Li, and S. G. Louie, Phys. Rev. Lett. **114**, 236602 (2015).
[10] H. L. Zhuang and R. G. Hennig, Phys. Rev. B **93**, 054429 (2016).
[11] Y. Ma, Y. Dai, M. Guo, C. Niu, Y. Zhu, and B. Huang, ACS Nano **6**, 1695 (2012).
[12] E. B. Isaacs and C. A. Marianetti, Phys. Rev. B **94**, 035120 (2016).
[13] M. Kan, B. Wang, Y. H. Lee, and Q. Sun, Nano Res. **8**, 1348 (2015).

[14] H.-R. Fuh, C.-R. Chang, Y.-K. Wang, R. F. L. Evans, R. W. Chantrell, and H.-T. Jeng, Sci. Rep. **6**, 32625 (2016).
[15] P.-R. Huang, Y. He, H. K. Pal, and M. Kindermann, arXiv:1501.00760.
[16] T. Wang, Y. Li, C. Xia, X. Zhao, Y. An, and X. Dai, J. Mater. Chem. C **4**, 8111 (2016).
[17] A. K. Geim and I. V. Grigorieva, Nature (London) **499**, 419 (2013).
[18] Y. Deng, Z. Luo, N. J. Conrad, H. Liu, Y. Gong, S. Najmaei, P. M. Ajayan, J. Lou, X. Xu, and P. D. Ye, ACS Nano **8**, 8292 (2014).
[19] M. M. Furchi, A. Pospischil, F. Libisch, J. Burgdrfer, and T. Mueller, Nano Lett. **14**, 4785 (2014).
[20] X. Zhang, F. Meng, J. R. Christianson, C. Arroyo-Torres, M. A. Lukowski, D. Liang, J. R. Schmidt, and S. Jin, Nano Lett. **14**, 3047 (2014).
[21] A. Suslu, K. Wu, H. Sahin, B. Chen, S. Yang, H. Cai, T. Aoki, S. Horzum, J. Kang, F. M. Peeters, and S. Tongay, Sci. Rep. **6**, 20525 (2016).
[22] M. Yagmurcukardes, E. Torun, R. T. Senger, F. M. Peeters, and H. Sahin, Phys. Rev. B **94**, 195403 (2016).
[23] P. E. Blöchl, Phys. Rev. B **50**, 17953 (1994).
[24] G. Kresse and J. Furthmüller, Comput. Mater. Sci. **6**, 15 (1996).
[25] J. P. Perdew, K. Burke, and M. Ernzerhof, Phys. Rev. Lett. **77**, 3865 (1996).
[26] G. Kresse and J. Furthmüller, Phys. Rev. B **54**, 11169 (1996).
[27] H. J. Monkhorst and J. D. Pack, Phys. Rev. B **13**, 5188 (1976).
[28] S. Grimme, J. Comput. Chem. **27**, 1787 (2006).
[29] T. Kerber, M. Sierka, and J. Sauer, J. Comput. Chem. **29**, 2088 (2008).
[30] J. Heyd and G. E. Scuseria, J. Chem. Phys. **121**, 1187 (2004).
[31] J. Heyd, J. E. Peralta, G. E. Scuseria, and R. L. Martin, J. Chem. Phys. **123**, 174101 (2005).
[32] N. Lu, H. Guo, L. Li, J. Dai, L. Wang, W.-N. Mei, X. Wu, and X. C. Zeng, Nanoscale **6**, 2879 (2014).
[33] See Supplemental Material at http://link.aps.org/supplemental/10.1103/PhysRevB.95.245408 for the structural parameters, band structures of monolayers, and different stacking patterns of heterostructures.
[34] A. H. M. A. Wasey, S. Chakrabarty, and G. P. Das, J. Appl. Phys. **117**, 064313 (2015).
[35] J. Zhou, Q. Wang, Q. Sun, and P. Jena, Phys. Rev. B **81**, 085442 (2010).
[36] X. Zhang, Z. Meng, D. Rao, Y. Wang, Q. Shi, Y. Liu, H. Wu, K. Deng, H. Liu, and R. Lu, Energy Environ. Sci. **9**, 841 (2016).
[37] W. Hu, T. Wang, R. Zhang, and J. Yang, J. Mater. Chem. C **4**, 1776 (2016).
[38] M. Rodriguez-Vega, J. Fischer, S. Das Sarma, and E. Rossi, Phys. Rev. B **90**, 035406 (2014).
[39] W. Xiong, C. Xia, X. Zhao, T. Wang, and Y. Jia, Carbon **109**, 737 (2016).
[40] R. A. de Groot, F. M. Mueller, P. G. van Engen, and K. H. J. Buschow, Phys. Rev. Lett. **50**, 2024 (1983).
[41] H. van Leuken and R. A. de Groot, Phys. Rev. Lett. **74**, 1171 (1995).
[42] S. O. Koswatta, S. J. Koester, and W. Haensch, IEEE Trans. Electron Dev. **57**, 3222 (2010).
[43] Y. Lee, Y. Hwang, and Y.-C. Chung, ACS App. Mater. Interf. **7**, 7163 (2015).
[44] R. Yan, S. Fathipour, Y. Han, B. Song, S. Xiao, M. Li, N. Ma, V. Protasenko, D. A. Muller, D. Jena, and H. G. Xing, Nano Lett. **15**, 5791 (2015).
[45] M. Z. Bellus, M. Li, S. D. Lane, F. Ceballos, Q. Cui, X. C. Zeng, and H. Zhao, Nanoscale Horiz. **2**, 31 (2017).
[46] Z. H. Lu, D. J. Lockwood, and J.-M. Baribeau, Nature (London) **378**, 258 (1995).
[47] S. Rathi, I. Lee, D. Lim, J. Wang, Y. Ochiai, N. Aoki, K. Watanabe, T. Taniguchi, G.-H. Lee, Y.-J. Yu, P. Kim, and G.-H. Kim, Nano Lett. **15**, 5017 (2015).
[48] Y. Yu, S. Hu, L. Su, L. Huang, Y. Liu, Z. Jin, A. A. Purezky, D. B. Geohegan, K. W. Kim, Y. Zhang, and L. Cao, Nano Lett. **15**, 486 (2015).
[49] K. Liu, Q. Yan, M. Chen, W. Fan, Y. Sun, J. Suh, D. Fu, S. Lee, J. Zhou, S. Tongay, J. Ji, J. B. Neaton, and J. Wu, Nano Lett. **14**, 5097 (2014).
[50] K. Dolui, I. Rungger, and S. Sanvito, Phys. Rev. B **87**, 165402 (2013).
[51] Y. y. Wang, Z. h. Ni, T. Yu, Z. X. Shen, H. m. Wang, Y. h. Wu, W. Chen, and A. T. Shen Wee, J. Phys. Chem. C **112**, 10637 (2008).